Spark plasma sintering grain growth assessment by densification kinetics analysis

Charles Manière, Joseph Sambasene Diatta, Christophe Couder, Christelle Harnois, Sylvain Marinel

Spark plasma sintering grain growth assessment by densification kinetics analysis

Charles Manière[1*], Joseph Sambasene Diatta[2*], Christophe Couder[1], Christelle Harnois[1], Sylvain Marinel[1],

1 Normandie Univ, ENSICAEN, UNICAEN, CNRS, CRISMAT, 14000 Caen, France

2 Assane Seck University, Ziguinchor, Sénégal

* charles.maniere@ensicaen.fr ; jsdiatta@univ-zig.sn

Abstract:

Modeling the spark plasma sintering of ceramics can be a very time-consuming task requiring high temperature sintering tests with fully dense/porous specimens in different configurations. Final stage sintering requires a particular attention as the densification kinetic is closely related to the grain growth phenomenon. In this work, we describe a combined master sintering curve and regression method which is able to determine all sintering model parameters. The original approach of this study lies in the possibility to estimate the grain size curve with the grain growth disturbance on the densification kinetics at the final stage. The model and grain size curve estimation reproduce well the experimental data points.

Keywords: Spark Plasma Sintering; Grain growth; Alumina; Modeling

Graphical Abstract:

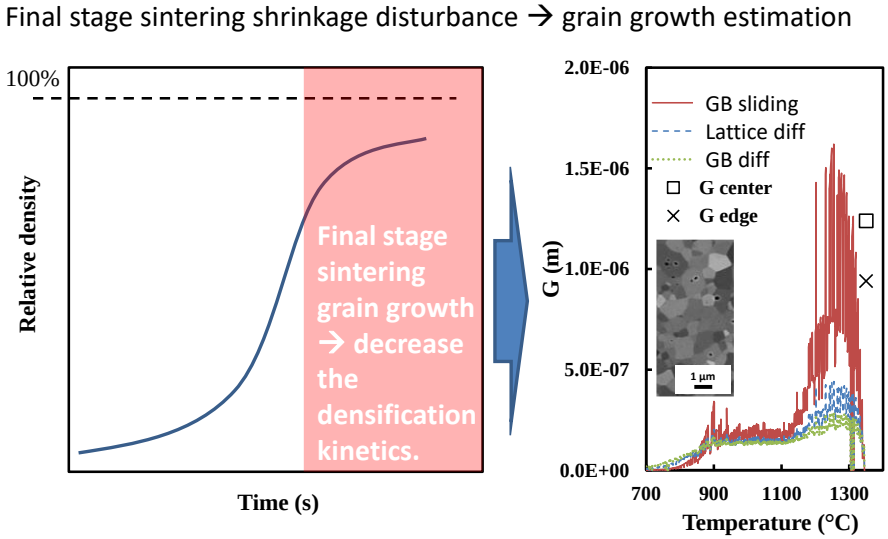

Nomenclature

θ Porosity
ρ Realtive density
$\dot{\theta}$ Porosity elimination rate (s^{-1})
σ_z Applied stress ($N.m^{-2}$)
n Creep law stress exponent
A Creep law deformability term ($s^{-1}.Pa^{-n}$)
A_0 Creep pre-exponential factor ($K.s^{-1}.Pa^{-n}$)
m Creep law grain size sensitivity exponent
Q Sintering activation energy ($J.mol^{-1}$)
R Gas constant 8.314 ($J.mol^{-1}.K^{-1}$)
T Temperature (K)
φ Shear modulus
ψ Bulk modulus
P_l Sintering stress (Pa)
$\dot{G}$ Grain growth rate ($m.s^{-1}$)
G Grain size (m)
G_0 Initial grain size (m)
K Grain growth factor ($m^{1+p}.s^{-1}$)
k_0 Grain growth pre-exponential factor ($m^{1+p}.s^{-1}$)
Q_G Grain growth activation energy ($J.mol^{-1}$)

Spark Plasma Sintering (SPS) is a pressure assisted sintering process involving high heating rates (~100 K/min) and external applied pressure (50-100 MPa)[1–6]. With these conditions, the sintering of ceramics takes place in a few minutes or even a few seconds in flash SPS conditions[7,8]. SPS is very efficient to eliminate the porosity[9] and decrease the sintering temperature which significantly limits the grain growth compared to conventional sintering[10,11].

The modeling of SPS sintering of ceramic is a challenge requiring determining the temperature/pressure dependent creep behavior, the sintering shear and bulk moduli and the final stage sintering grain growth[12,13]. The identification of all these parameters can be very time consuming because it requires high temperature sintering tests on fully dense and porous samples in different configurations[14–22]. It is difficult to identify independently the creep behavior without the grain growth disturbance of the final stage. A solution has been developed to determine the moduli from instrumented sinter-forging tests but this requires a lot of tests[23]. Direct regression approaches exist to identify the sintering behavior directly from the densification curve. However, such approaches require using theoretical hypotheses on the sintering moduli with values often far from the real grains structures behavior. [24,25]. Moreover, unlike zirconia that has a very limited grain growth, alumina final stage sintering is strongly influenced by grain growth[26]. In a previous work, we show that taking into account the grain growth in the model is mandatory to reproduce realistic final stage relative density where the grain growth significantly decreases the densification kinetics[27]. Previously, we show (on conventional sintering of zirconia) that combining a master sintering curve study with an inverse approach, it is possible to calibrate the experimental moduli and estimate the final stage sintering grain growth simply with the final stage dilatometry densification behavior[28]. The obtained final grain size was very close to the experimental one verified by electron microscopy. In this work, the SPS sintering equations are adapted to apply the same grain growth estimation method when pressure is applied. In this method (applied to SPS rather than conventional sintering) a master sintering curve (MSC)[29] is first conducted for providing a fixed sintering activation energy used as a reference point to adjust the shear and bulk moduli *via* a linear regression. Then, like for conventional sintering, the final stage sintering non-linear discrepancies are used to estimate the grain growth curves which explain these discrepancies.

An SPS device SPS FCT HP25 with a binderless 0.12µm Baikowski BMA15 alumina powder was used. A master sintering curve study has been done with three sintering tests at 100, 50 and 20K/min at 50MPa up to 1350°C. The sintering modeling method consists of four stages.

(i) In the first stage, the sintering activation energy is identified by the master sintering curve method[29].

(ii) In the next step, Skorohod-Olevsky SPS equation is used[23]:

$$-\frac{1}{\rho}\frac{d\rho}{dt} = A(T,G)\left(\psi+\frac{2}{3}\varphi\right)^{\frac{-n-1}{2}}(1-\theta)^{\frac{1-n}{2}}(\sigma_z - P_l)^n \quad (1)$$

In the region of inactive grain growth, the term $A(T) = \frac{A_0}{T}exp\left(\frac{-Q}{RT}\right)$ can be isolated in (1). Then, with $\dot{\rho} = -\dot{\theta}$ and taking the logarithm, equation (1) gives the following regression equation Y *vs* (1/RT):

$$Y = ln\left(T\left|\dot{\theta}\right|\left|\sigma_z - P_l\right|^{-n}\left(\psi+\frac{2}{3}\varphi\right)^{\frac{n+1}{2}}(1-\theta)^{\frac{n-3}{2}}\right) = ln(A_0) - \frac{Q}{RT} \quad (2)$$

In the latter, the value of n=2.3 is known from a previous SPS test between 1000 and 1100°C[30]. Because the activation energy (Q) is known from the master sintering curve, it is possible to correct the Skorohod[31] theoretical moduli *via* the unknown parameters a,b,c,θ_{cr} ($\psi = a\frac{(\theta_{cr}-\theta)^b}{\theta^c}$ & $\varphi = \left(1-\frac{\theta}{\theta_{cr}}\right)^2$) to impose the slope of the known activation energy (MSC). It is important to conduct this adjustment in the open porosity zone where the grain growth is not active as linear deviations appear in the final stage due to the grain growth disturbances. After the adjustment of the moduli, the A_0 is obtained by the origin value of the regression curve ($exp(A_0)$).

(iii) Knowing all the densification parameters in inactive grain growth zone, it is possible to estimate the grain growth in the final stage with the following equation.

$$G = \left(\frac{T}{A_0 G_0^m}exp\left(\frac{Q}{RT}\right)\left|\dot{\theta}\right|\left|\sigma_z - P_l\right|^{-n}\left(\psi+\frac{2}{3}\varphi\right)^{\frac{n+1}{2}}(1-\theta)^{\frac{n-3}{2}}\right)^{-\frac{1}{m}} \quad (3)$$

Three grain size curves are estimated assuming grain boundary sliding (m=1 by dislocation motion adjacent to the grain boundary[32,33]), lattice diffusion (m=2) and grain boundary diffusion (m=3). These mechanisms are typically cited for hot pressing models[34].

However, grain boundary sliding has 9 different mechanisms with m=1-3[32] so, in this study, we mainly analyze the grain size sensitivity (m) of the model.

From, these three results and taking the grain size curves that better explain the final grain sizes, it is possible to calculate an estimated normal grain growth law by the following regression.

$$ln\left(\dot{G}G^2\right) = ln(K_0) - \frac{Q_G}{RT} \quad (4)$$

(iv) Finally, knowing all model densification parameters and with a final stage estimated grain growth behavior. It is possible to simulate with (1) the three SPS tests to verify if the model fits well the experimental data point. At this stage, a slight adjustment in the fitted regression model (in equation (2) and (4)) can be done to obtain a model as close as possible to the experiment.

In the following, the stages (i) to (iv) are presented and described.

The densification curves obtained by SPS sintering and for three heating rates are shown in **Figure 2 (A)**. Typically, we can observe a shift towards lower sintering temperature for lower heating rates. **Figure 2 (B)** shows the relative density curve from the MSC study, and in the insert, the activation energy of 392 kJ/mol that was determined. This value obtained in this study is close to the 430kJ/mol[35] and the 487kJ/mol[30] obtained for a TMDAR alumina powder very close to the BMA15 powder of this study.

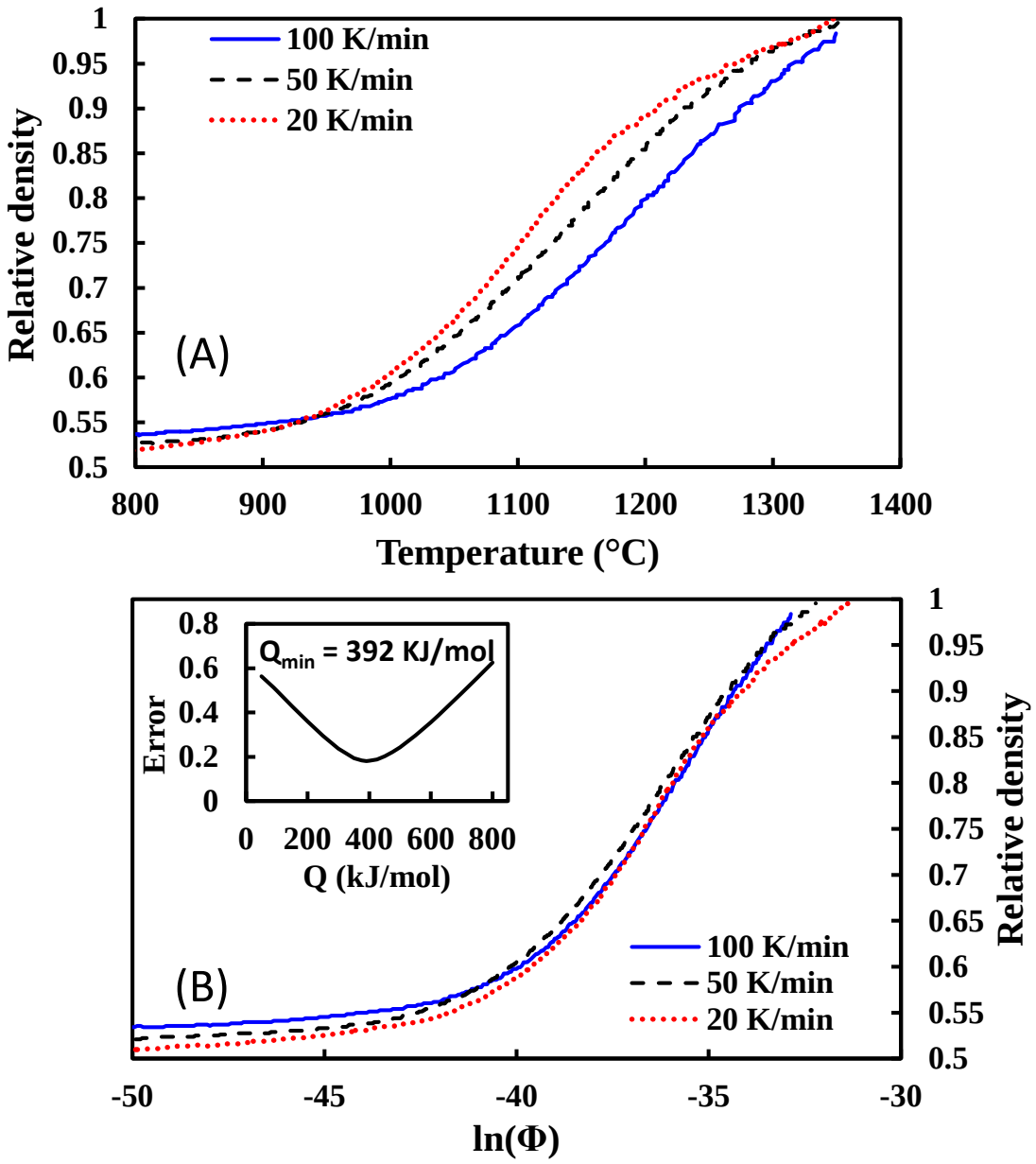

Figure 1. Relative density curves at constant heating rate of 20, 50 and 100K/min (A) and sintering activation energy identification by the Master Sintering Curve (B), in the inset, the minimization study showing the three curves misfit called "error" is reported for each tested activation energy.

In the next step (ii), the linear regression is conducted and the shear and bulk moduli are adjusted to obtain a slope that corresponds to the MSC Q value. **Figure 2** shows the results of the regression after the moduli adjustment with a fitted value of A_0 equal to $7.485E^{-5}$ m^3s^{-1}. This figure shows that the linear regression was performed on the initial and intermediate stages. The fitting parameters of the shear and bulk moduli are $\theta_{cr} = 0.51$, $a = 2/3$, $b = 3$ and $c = 1$. It can be seen in **Figure 2** that the linear regression is less accurate in the final stage of sintering, where grain growth occurs. This grain

growth disturbance in the final stage is precisely the phenomena exploited to estimate the grain growth in the next step of the study.

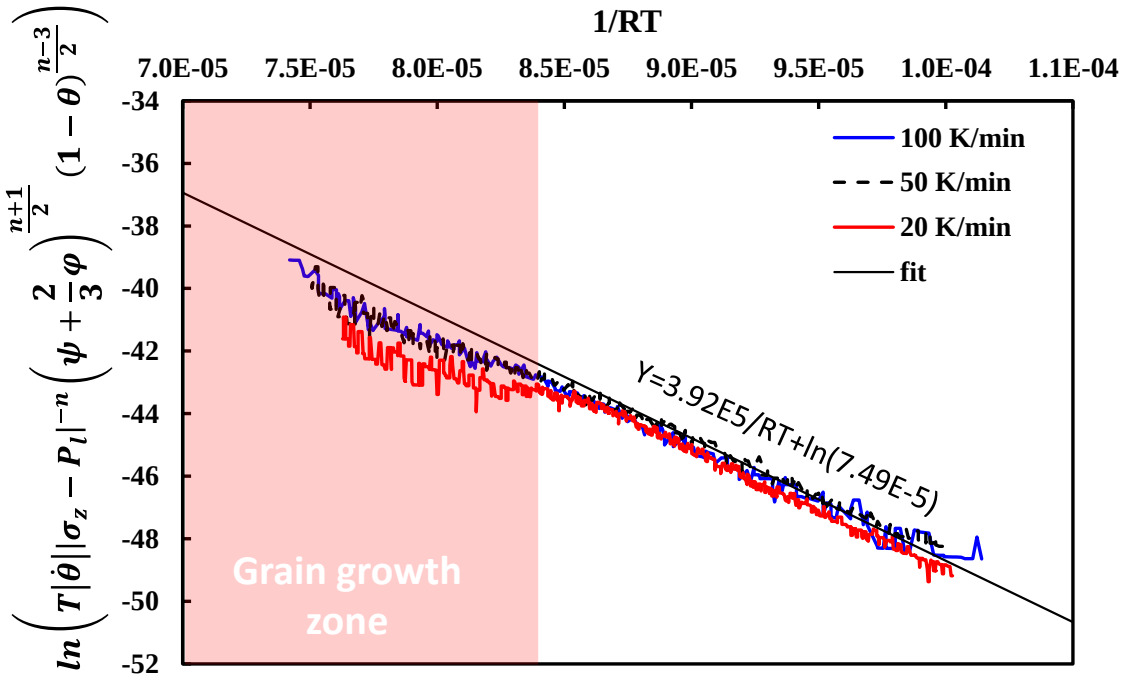

Figure 2. Regression analysis using SPS data for correction of the moduli and the identification of A_0 ; the red region is determined by identifying the disturbances of the initial linear behavior; here, the disturbance appears near 1400K and is associated with the grain growth influence on the densification kinetics.

Figure 3 shows the grain size results for each heating rate and for three probable mechanisms (grain boundary sliding, lattice/grain boundary diffusion m=1-3). To compare the 9 curves obtained from equation (3) with the final experimental grain size, scanning electron microscopy measurements were performed at two locations (center and edge) of the sintered samples. The grain size estimated from the model is relatively underestimated without being too far from the final grain sizes. Langdon's grain boundary sliding m=1[33] seems to correspond well to the experimental values as the other mechanisms underestimate more the final grain sizes. Grain boundary sliding is also a relevant mechanism with the stress exponent of n=2.3 used for this powder[34].

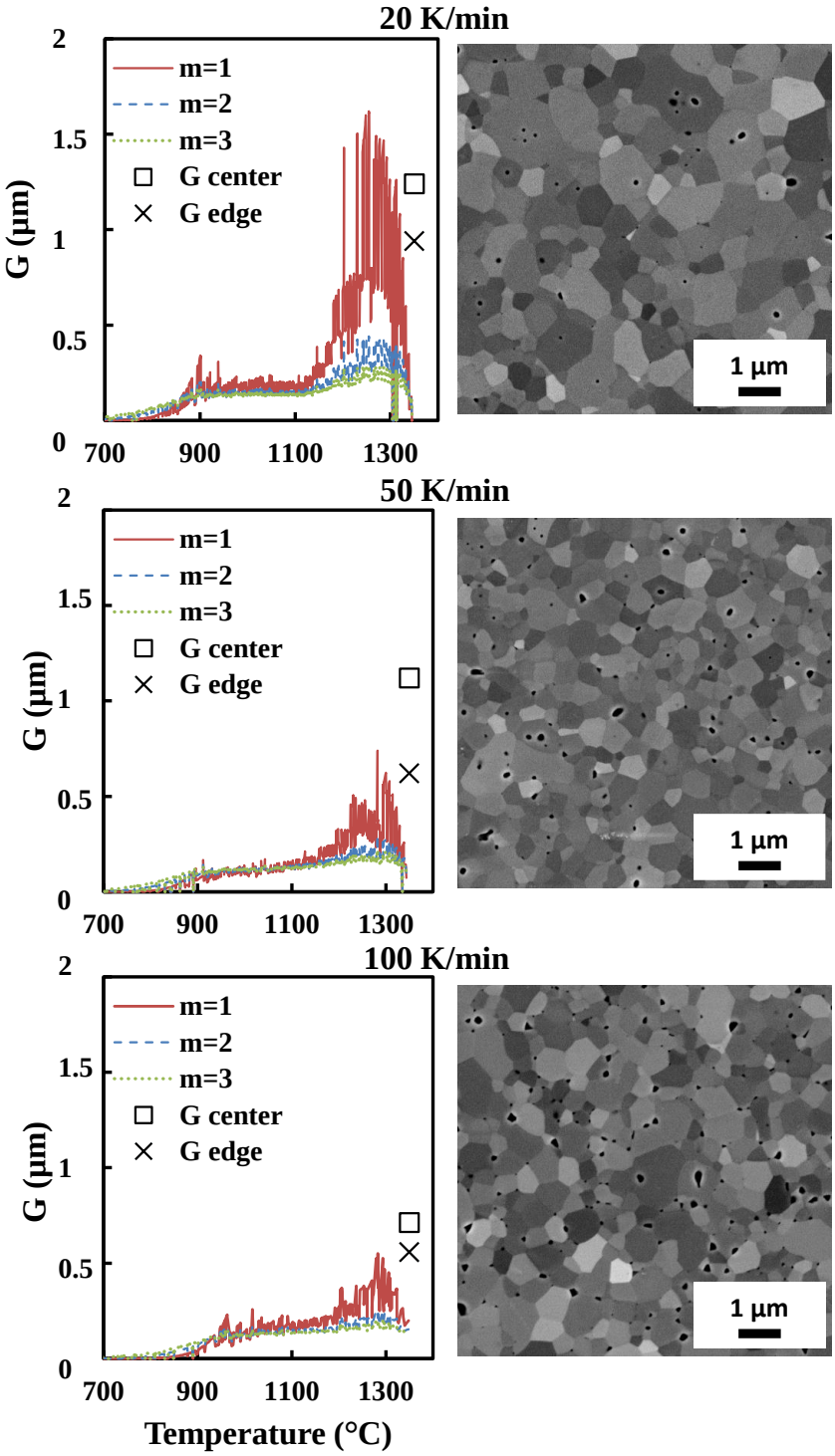

Figure 3. Estimated grain size as a function of temperature when lattice diffusion (m=2), grain–boundary-diffusion (m=3) or grain–boundary-sliding mechanism (m=1) is assumed.

From the estimated grain size curves of grain boundary sliding (m=1), the regression equation (4) is calculated to identify the grain growth activation energy (Q_G) and pre-exponent coefficient (K_0). The result is reported in **figure 4 (A)**. The method is applied only to the final stage of sintering. The values obtained for Q_G and k_0 are 196 kJ/mol and $1.04E^{-16}$ m^3s^{-1}, respectively. The literature grain growth

activation energy is closer to 443 kJ/mol[36] for alumina. However, the identified behavior represents the early stage of grain growth which may behave differently from the fully dense ceramic grain growth. Porosity pinning[37–39] or dynamic grain growth[40,41] may occur involving different grain growth behaviors in the initial stage so the identified behavior is an empirical law aimed at correcting the final stage sintering modeled densification curves.

To verify the model, the experimental densification curves are compared with the simulated sintering curves with and without grain growth in **Figure 4 (B)**. The analytical sintering models highlight the importance of grain growth in the final stage. When the phenomenon of grain growth in the final stage is neglected, the model is unable to reproduce the reduction of the sintering kinetics of the final stage. On the contrary, the comprehensive model (with grain growth) corrects the final stage sintering densification behavior which fit well all the modeled SPS curves.

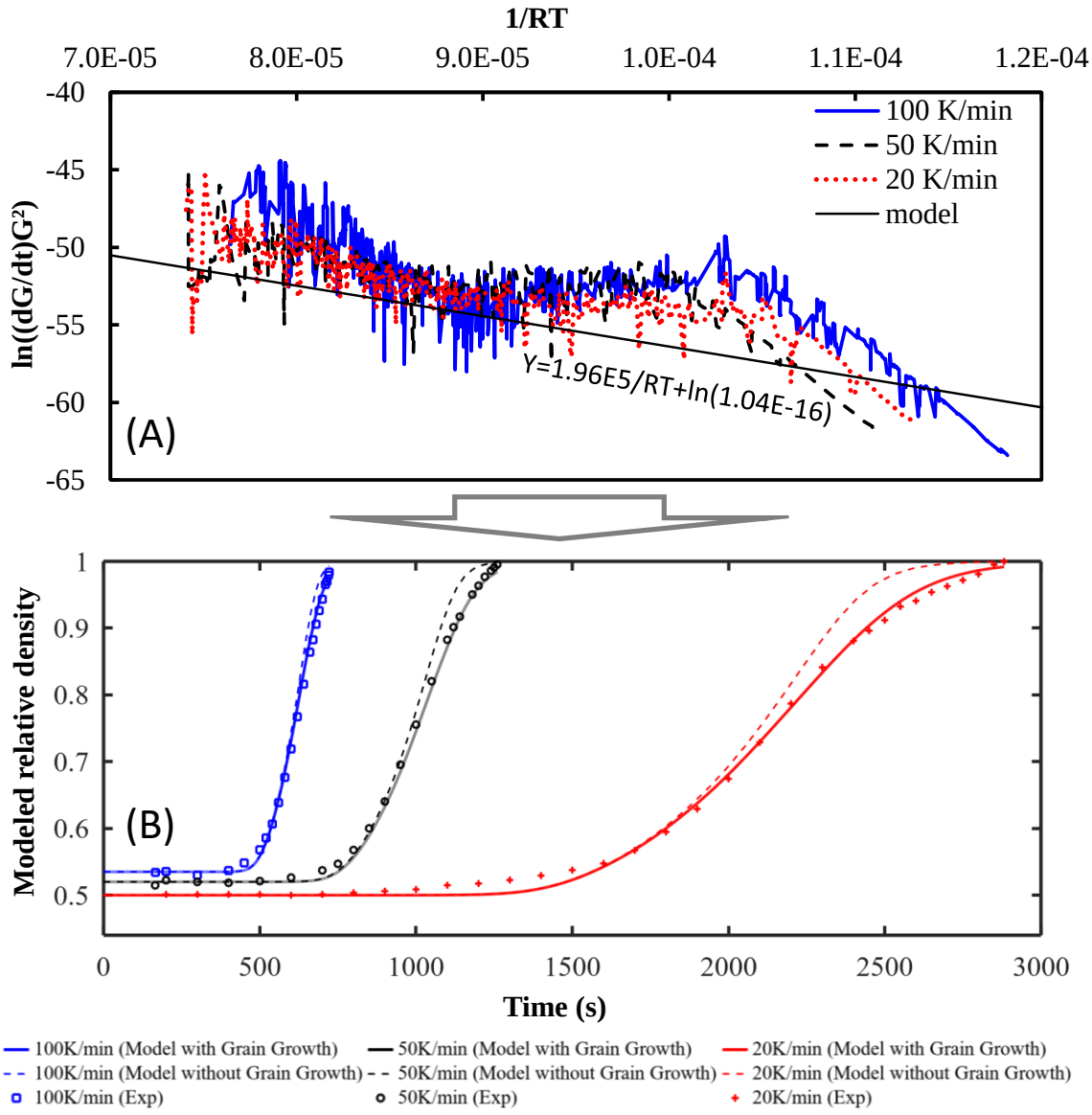

Figure 4. Identification of grain growth model based on grain boundary sliding mechanism (A), simulated and experimental relative density curves vs time for the different heating rates (B).

To conclude, this study presents a comprehensive model of alumina spark plasma sintering taking into account the densification and the grain growth. The assessment of the modeling parameters has been done by a combination of the master sintering curve and the Skorohod-Olevsky model. Based on the perturbation of the densification kinetics by the grain growth, an original approach capable of estimating the grain size curve from sintering shrinkage has been developed. The spark plasma sintering model and the estimated grain size curves approach reproduce well the experiments.

The interesting aspect of this approach is the possibility to determine both the sintering model parameters and the microstructure development with minimal experimental data and reasonable model hypotheses. The obtain modeling parameters are implementable in a simulation code.

Acknowledgments

The help and support of Christelle Bilot and Jérôme Lecourt is gratefully acknowledged. This work was supported by: the French National Research Agency (ANR), project ULTRARAPIDE N°ANR-19-CE08-0033-01 and the project "région normandie" - 00016601-20E02057_RIN RECHERCHE 2020 - Emergent – ULTIMODULUS.

References

[1] O. Guillon, J. Gonzalez-Julian, B. Dargatz, T. Kessel, G. Schierning, J. Räthel, M. Herrmann, Field-Assisted Sintering Technology/Spark Plasma Sintering: Mechanisms, Materials, and Technology Developments, Adv. Eng. Mater. 16 (2014) 830–849. doi:10.1002/adem.201300409.

[2] R. Orrù, R. Licheri, A.M. Locci, A. Cincotti, G. Cao, Consolidation/synthesis of materials by electric current activated/assisted sintering, Mater. Sci. Eng. R Reports. 63 (2009) 127–287. doi:10.1016/j.mser.2008.09.003.

[3] S.H. Risbud, Y.-H. Han, Preface and historical perspective on spark plasma sintering, Scr. Mater. 69 (2013) 105–106. doi:10.1016/j.scriptamat.2013.02.024.

[4] W. Chen, U. Anselmi-Tamburini, J.E. Garay, J.R. Groza, Z.A. Munir, Fundamental investigations on the spark plasma sintering/synthesis process, Mater. Sci. Eng. A. 394 (2005) 132–138. doi:10.1016/j.msea.2004.11.020.

[5] G. Cao, C. Estournès, J.E. Garay, R. Orrù, Spark Plasma Sintering, Elsevier, Elsevier, 2019. doi:10.1016/C2018-0-02428-7.

[6] E.A. Olevsky, D. V. Dudina, Field-Assisted Sintering, Springer N, Springer International Publishing, Cham, 2018. doi:10.1007/978-3-319-76032-2.

[7] M. Yu, S. Grasso, R. Mckinnon, T. Saunders, M.J. Reece, Review of flash sintering: materials, mechanisms and modelling, Adv. Appl. Ceram. 116 (2017) 24–60. doi:10.1080/17436753.2016.1251051.

[8] M. Biesuz, V.M. Sglavo, Flash sintering of ceramics, J. Eur. Ceram. Soc. 39 (2019) 115–143. doi:10.1016/j.jeurceramsoc.2018.08.048.

[9] D. Jiang, D.M. Hulbert, U. Anselmi-Tamburini, T. Ng, D. Land, A.K. Mukherjee, Optically Transparent Polycrystalline Al2O3 Produced by Spark Plasma Sintering, J. Am. Ceram. Soc. 91 (2007) 151–154. doi:10.1111/j.1551-2916.2007.02086.x.

[10] Z.-Y. Hu, Z.-H. Zhang, X.-W. Cheng, F.-C. Wang, Y.-F. Zhang, S.-L. Li, A review of multi-physical fields induced phenomena and effects in spark plasma sintering: Fundamentals and applications, Mater. Des. 191 (2020) 108662. doi:10.1016/j.matdes.2020.108662.

[11] T. Herisson de Beauvoir, A. Sangregorio, I. Cornu, C. Elissalde, M. Josse, Cool-SPS: an opportunity for low temperature sintering of thermodynamically fragile materials, J. Mater. Chem. C. 6 (2018) 2229–2233. doi:10.1039/C7TC05640K.

[12] E.A. Olevsky, Theory of sintering: from discrete to continuum, Mater. Sci. Eng. R Reports. 23 (1998) 41–100. doi:10.1016/S0927-796X(98)00009-6.

[13] R.K. Bordia, S.-J.L. Kang, E.A. Olevsky, Current understanding and future research directions at the onset of the next century of sintering science and technology, J. Am. Ceram. Soc. 100 (2017) 2314–2352. doi:10.1111/jace.14919.

[14] M. Abouaf, PhD, Modélisation de la compaction de poudres métalliques frittées, approches par la mécanique des milieux continus, Institut national polytechnique de Grenoble, 1985.

[15] J. Besson, M. Abouaf, Rheology of Porous Alumina and Simulation of Hot Isostatic Pressing, J. Am. Ceram. Soc. 75 (1992) 2165–2172. doi:10.1111/j.1151-2916.1992.tb04479.x.

[16] C. Nicolle, PhD, Mise en forme de poudre de bore par compression isostatique à chaud: determination des propriétés rhéologiques et simulation numérique du procédé, Université de Bourgogne, France, 1999.

[17] C. Geindreau, D. Bouvard, P. Doremus, Constitutive behaviour of metal powder during hot forming. Part I: Experimental investigation with lead powder as a simulation material, Eur. J.

Mech. - A/Solids. 18 (1999) 581–596. doi:10.1016/S0997-7538(99)00102-3.

[18] C. Wolff, S. Mercier, H. Couque, A. Molinari, F. Bernard, F. Naimi, Thermal-electrical-mechanical simulation of the nickel densification by Spark Plasma Sintering. Comparison with experiments, Mech. Mater. 100 (2016) 126–147. doi:10.1016/j.mechmat.2016.06.012.

[19] Y. Xue, L.H. Lang, G.L. Bu, L. Li, Densification modeling of titanium alloy powder during hot isostatic pressing, Sci. Sinter. 43 (2011) 247–260. doi:10.2298/SOS1103247X.

[20] C. Manière, U. Kus, L. Durand, R. Mainguy, J. Huez, D. Delagnes, C. Estournès, Identification of the Norton-Green Compaction Model for the Prediction of the Ti-6Al-4V Densification During the Spark Plasma Sintering Process, Adv. Eng. Mater. 18 (2016) 1720–1727. doi:10.1002/adem.201600348.

[21] D. Martins, F. Grumbach, C. Manière, P. Sallot, K. Mocellin, M. Bellet, C. Estournès, In-situ creep law determination for modeling Spark Plasma Sintering of TiAl 48-2-2 powder, Intermetallics. 86 (2017) 147–155. doi:10.1016/j.intermet.2017.03.006.

[22] C. Manière, E.A. Olevsky, Porosity dependence of powder compaction constitutive parameters: Determination based on spark plasma sintering tests, Scr. Mater. 141 (2017) 62–66. doi:10.1016/j.scriptamat.2017.07.026.

[23] C. Manière, C. Harnois, S. Marinel, Porous stage assessment of pressure assisted sintering modeling parameters: a ceramic identification method insensitive to final stage grain growth disturbance, Acta Mater. 211 (2021) 116899. doi:10.1016/j.actamat.2021.116899.

[24] G. Bernard-Granger, C. Guizard, Spark plasma sintering of a commercially available granulated zirconia powder: I. Sintering path and hypotheses about the mechanism(s) controlling densification, Acta Mater. 55 (2007) 3493–3504. doi:10.1016/j.actamat.2007.01.048.

[25] C. Manière, L. Durand, G. Chevallier, C. Estournès, A spark plasma sintering densification modeling approach: from polymer, metals to ceramics, J. Mater. Sci. 53 (2018) 7869–7876. doi:10.1007/s10853-018-2096-8.

[26] C. Manière, L. Durand, A. Weibel, C. Estournès, A predictive model to reflect the final stage of spark plasma sintering of submicronic α-alumina, Ceram. Int. 42 (2016) 9274–9277.

doi:10.1016/j.ceramint.2016.02.048.

[27] C. Manière, L. Durand, A. Weibel, C. Estournès, Spark-plasma-sintering and finite element method: From the identification of the sintering parameters of a submicronic α -alumina powder to the development of complex shapes, Acta Mater. 102 (2016) 169–175. doi:10.1016/j.actamat.2015.09.003.

[28] C. Manière, T. Grippi, S. Marinel, Estimate microstructure development from sintering shrinkage: A kinetic field approach, Mater. Today Commun. 31 (2022) 103269. doi:10.1016/j.mtcomm.2022.103269.

[29] O. Guillon, J. Langer, Master sintering curve applied to the Field-Assisted Sintering Technique, J. Mater. Sci. 45 (2010) 5191–5195. doi:10.1007/s10853-010-4556-7.

[30] G. Antou, P. Guyot, N. Pradeilles, M. Vandenhende, A. Maître, Identification of densification mechanisms of pressure-assisted sintering: application to hot pressing and spark plasma sintering of alumina, J. Mater. Sci. 50 (2015) 2327–2336. doi:10.1007/s10853-014-8804-0.

[31] V.V. Skorohod, Rheological basis of the theory of sintering, Nauk. Dumka, Kiev. (1972).

[32] O.D. Sherby, J. Wadsworth, Superplasticity—Recent advances and future directions, Prog. Mater. Sci. 33 (1989) 169–221. doi:10.1016/0079-6425(89)90004-2.

[33] T.G. Langdon, Grain boundary sliding as a deformation mechanism during creep, Philos. Mag. 22 (1970) 689–700. doi:10.1080/14786437008220939.

[34] M.N. Rahaman, Sintering of Ceramics, CRC Press, 2007.

[35] J. Langer, M.J. Hoffmann, O. Guillon, Direct comparison between hot pressing and electric field-assisted sintering of submicron alumina, Acta Mater. 57 (2009) 5454–5465. doi:10.1016/j.actamat.2009.07.043.

[36] Y.S. Kwon, G. Son, J. Suh, K.T. Kim, Densification and Grain Growth of Porous Alumina Compacts, J. Am. Ceram. Soc. 77 (1994) 3137–3141. doi:10.1111/j.1151-2916.1994.tb04561.x.

[37] G. Kerbart, C. Manière, C. Harnois, S. Marinel, Predicting final stage sintering grain growth affected by porosity, Appl. Mater. Today. 20 (2020) 100759. doi:10.1016/j.apmt.2020.100759.

[38] E.A. Olevsky, C. Garcia-Cardona, W.L. Bradbury, C.D. Haines, D.G. Martin, D. Kapoor,

Fundamental Aspects of Spark Plasma Sintering: II. Finite Element Analysis of Scalability, J. Am. Ceram. Soc. 95 (2012) 2414–2422. doi:10.1111/j.1551-2916.2012.05096.x.

[39] J. Zhao, M.P. Harmer, Effect of Pore Distribution on Microstructure Development: III, Model Experiments, J. Am. Ceram. Soc. 75 (1992) 830–843. doi:10.1111/j.1151-2916.1992.tb04148.x.

[40] B.-N. Kim, K. Hiraga, K. Morita, H. Yoshida, Y.-J. Park, Y. Sakka, Dynamic grain growth during low-temperature spark plasma sintering of alumina, Scr. Mater. 80 (2014) 29–32. doi:10.1016/j.scriptamat.2014.02.015.

[41] J. Besson, M. Abouaf, Grain growth enhancement in alumina during hot isostatic pressing, Acta Metall. Mater. 39 (1991) 2225–2234. doi:10.1016/0956-7151(91)90004-K.